



Get Clarity On Generics

Cost-Effective CT & MRI Contrast Agents



FRESENIUS
KABI

WATCH VIDEO

AJNR

4D Flat Panel Conebeam CTA for Analysis of the Angioarchitecture of Cerebral AVMs with a Novel Software Prototype

F. Keil, A. Bergkemper, A. Birkhold, M. Kowarschik, S. Tritt and J. Berkefeld

This information is current as of August 8, 2025.

AJNR Am J Neuroradiol 2022, 43 (1) 102-109

doi: <https://doi.org/10.3174/ajnr.A7382>

<http://www.ajnr.org/content/43/1/102>

4D Flat Panel Conebeam CTA for Analysis of the Angioarchitecture of Cerebral AVMs with a Novel Software Prototype

F. Keil, A. Bergkemper, A. Birkhold, M. Kowarschik, S. Tritt, and J. Berkefeld



ABSTRACT

BACKGROUND AND PURPOSE: Time-resolved 3DRA (4D-DSA) and flat panel conebeam CTA are new methods for visualizing the microangioarchitecture of cerebral AVMs. We applied a 4D software prototype to a series of cases of AVMs to assess the utility of this method in relation to treatment planning.

MATERIALS AND METHODS: In 33 patients with AVMs, 4D volumes and flat panel conebeam CTA images were recalculated from existing 3D rotational angiography data. The multiplanar reconstructions were used to determine intranidal arteriovenous branching patterns, categorize them according to common classifications of AVM angioarchitecture, and compare the results with those from 2D-DSA.

RESULTS: 4D flat panel conebeam CTA showed angioarchitectural features equal to or better than those of 2D-DSA in 30 of 33 cases. In particular, the reconstructions helped in understanding the intranidal microvasculature. Fistulous direct arteriovenous connections with a low degree of arterial branching ($n=22$) could be distinguished from plexiform arterial networks before the transition to draining veins ($n=11$). We identified AVMs with a single draining vein ($n=20$) or multiple draining veins ($n=10$). Arteriovenous shunts in the lateral wall of the draining veins ($n=22$) could be distinguished from cases with increased venous branching and shunts between corresponding intranidal arteries and veins ($n=11$). Limitations were the time-consuming postprocessing and the difficulties in correctly tracing intranidal vessels in larger and complex AVMs.

CONCLUSIONS: 4D flat panel conebeam CTA reconstructions allow detailed analysis of the nidus angioarchitecture of AVMs. However, further improvements in temporal resolution and automated reconstruction techniques are needed to use the method generally in clinical practice.

ABBREVIATIONS: AV = arteriovenous; CB = conebeam; fP = flat panel; 3DRA = 3D rotational angiography

Embolization as an interventional treatment option for cerebral AVMs requires a detailed understanding and accurate classification of the angioarchitecture of the nidus and its arterial and venous environment. On the basis of angiographic findings, we can separate arterial feeders from the nidus and the draining veins. MR imaging can show the anatomic location of the AVM and help to differentiate a compact from a diffuse nidus with normal brain tissue between the malformed vessels.


Arterial branches terminating in the nidus are distinguished from small feeders as side branches of arteries passing the nidus and supplying the brain parenchyma beyond.^{1,2} Concerning the intranidal branching patterns, direct fistulous transitions between arteries and draining veins are differentiated from plexiform arterial networks before the shunt zone.^{1,3} Single or multiple draining veins connected with the superficial or deep venous system are described as well as features like high flow (shunt volume), varicose enlargement, or stenosis of the draining veins. Perinidal arterial networks are regarded as separate from the nidus. Pre-, intranidal, or venous aneurysms could be associated with the AVM.^{2,4-6}

Most of these angioarchitectural features are detectable by means of 2D-DSA with high spatial and temporal resolution. However, overlapping vessels on DSA projection images may obscure details of the intranidal microvasculature. Vessel overlaid on projection images can be reduced by superselective angiography after catheterization of the nidus with a microcatheter. Due

Received June 11, 2021; accepted after revision September 22.

From the Institute of Neuroradiology (F.K., A. Bergkemper., J.B.), University of Frankfurt, Frankfurt, Germany; Siemens Healthcare (A. Birkhold, M.K.), Forchheim, Germany; Advanced Therapies (A. Birkhold, M.K.), Siemens Healthcare, Forchheim, Germany; and Helios Dr. Horst Schmidt Kliniken Wiesbaden (S.T.), Wiesbaden, Germany.

Please address correspondence to Fee Keil, MD, Institute of Neuroradiology, University Hospital of Frankfurt am Main, Schleusenweg 2-16, D-60528 Frankfurt am Main, Germany; e-mail: Fee.Keil@kgu.de

 Indicates article with online supplemental data.

<http://dx.doi.org/10.3174/ajnr.A7382>

to its invasiveness and need for general anesthesia, superselective angiography is hardly applicable for pretherapeutic diagnostic purposes. In most instances, it is used during embolization procedures immediately before the injection of embolic agents.⁴

Since the A Randomised Trial of Unruptured Brain Arteriovenous Malformations (ARUBA) proved high complication rates of AVM therapy,⁷ we have to ask whether our pretherapeutic understanding of AVM anatomy is good enough for planning safe and effective treatment. With increasing efficacy of embolic agents like Onyx (Covidien) for transarterial or transvenous AVM embolizations, exact visualization of the transition zone between arteries and veins in different nidal compartments becomes essential to achieve a controlled occlusion of the shunt. Accidental occlusion of arteries supplying normal brain or occlusion of the draining vein without control over the arterial part of the nidus must be avoided.⁸

There is a lack of publications concerning clear pathoanatomic descriptions of the intranidal microvasculature. Considerable disagreement between different reviewers concerning the extent and type of the nidus has been described.⁹ On the basis of MR imaging and DSA, current grading systems use rather simple criteria without detailed analysis of the angioarchitecture.^{10,11}

According to the described limitations of DSA and superselective angiography, we have to think about new imaging approaches: 3D rotational angiography (3DRA) and derived flat panel CT reconstructions, MR imaging, MRA, and CTA have no temporal resolution, and anatomic details may be missed due to overlapping of arteries and veins. In a pilot study, we showed that multiplanar reconstructions from time-resolved 3DRA (4D-DSA) data sets may have the potential for more detailed analysis of arteriovenous (AV) shunts.¹²

Use of a new software prototype for 4D reconstruction promised an improved visualization of the consecutive filling of arteries and veins. It was the aim of this study to analyze a variety of AVMs to determine whether 4D-DSA and flat panel conebeam CTA (4D-fPCBCTA) reconstructions with the novel software prototype could better visualize angioarchitectonic features of AVMs. Furthermore, we wanted to know whether 4D findings met the above-mentioned AVM classification criteria and to discuss the additional value for treatment planning compared with 2D-DSA.

MATERIALS AND METHODS

The novel software prototype was used to recalculate 4D-DSA volumes and 4D-fPCBCTA reconstructions from existing 3DRA data sets obtained during diagnostic angiography of patients with AVMs, which was part of our routine protocol for diagnostic work-up. The study protocol was approved by ethics committee of the Department of Medicine, University Hospital of the Goethe University.

For this retrospective study, we analyzed 38 data sets of consecutive patients with cerebral pial AVMs and indications for pretherapeutic 3DRA obtained between 2016 and 2019. All 4D reconstructions with sufficient image quality were included into this study. We excluded data sets with movement artifacts ($n = 3$) or incomplete examinations ($n = 2$).

3DRA was obtained on a modified Artis zee biplane angiography system (Siemens) using an increased 260° rotation angle of the frontal C-arm during a scan time of 12 seconds, which is intended to capture both arterial inflow and venous outflow. Acquisition consisted of 2 runs (a native run without contrast and a fill run with contrast) with 304 projection (0.85°/frame) images. In the second run, an x-ray delay of 2 seconds after automatic injection of a bolus of 20 mL of nonionic contrast material (iopromide, Ultravist 300; Bayer HealthCare) with a flow of 3 mL/s was used.

4D reconstructions (time-resolved 3D-DSA, 4D-DSA) were calculated after digital subtraction on a dedicated workstation (syngo X Workplace VD20; Siemens) with the use of a new software prototype developed by Siemens, comprising an additional postprocessing step compared with a version described in a first pilot study.¹² In this step, a physically motivated, plausibility-based flow constraint on the 4D reconstruction process required that a certain vessel segment can only be contrast-enhanced under certain conditions to reduce artifacts of incorrect/nonphysiologic vessel enhancement (due to vascular overlap).

4D-DSA uses the temporal information of 3DRA for reconstruction of 3D volumes at any given time point during the scan time. For evaluation and comparison with 2D-DSA, we used volume-rendering data sets with a display of virtual DSA images in arbitrary projections including a “working projection” showing the best feeding arteries, nidus, and draining veins (Fig 3). To reduce the overlay, we analyzed multiplanar reconstructions in 3 standard planes (coronal, sagittal, transversal) and a working projection to demonstrate intranidal, arterial, and venous branching patterns. Section thicknesses were chosen between 2.5 and 6.5 mm, depending on vessel diameters and degree of branching at the transition zone to the draining veins. The time points with the best display of intranidal vessels and veins were selected according to a cine loop of 100 reconstructed 3D volumes during the scan time. Assessment of the arterial part was favorable during the first 3 seconds; display of the veins was best at the end of the loop.

To determine the anatomic location of the AVM, we used MR imaging or fusion images between 4D-fPCBCTA reconstructions and MR imaging.¹³

We started the analysis with evaluation of 4D-fPCBCTA findings without consideration of 2D-DSA images or reports. Comparison with 2D-DSA images was performed in a second step without additional consideration of 3D-fPCBCTA reconstructions. All data sets, including 2D-DSA, were re-evaluated by a consensus by 2 reviewers.

The AVMs were characterized by following criteria:

- Anatomic location: superficial, deep, posterior fossa; sulcal, parenchymal, mixed
- Size of the nidus: $\leq 3/\leq 6$ cm / > 6 cm
- Venous drainage: superficial/deep
- Spetzler-Martin grade
- Rupture status.

Angioarchitectonic features were evaluated according to 4D volumes and 4D-fPCBCTA data:

- Arterial feeders: number, terminal, en passage, mixed

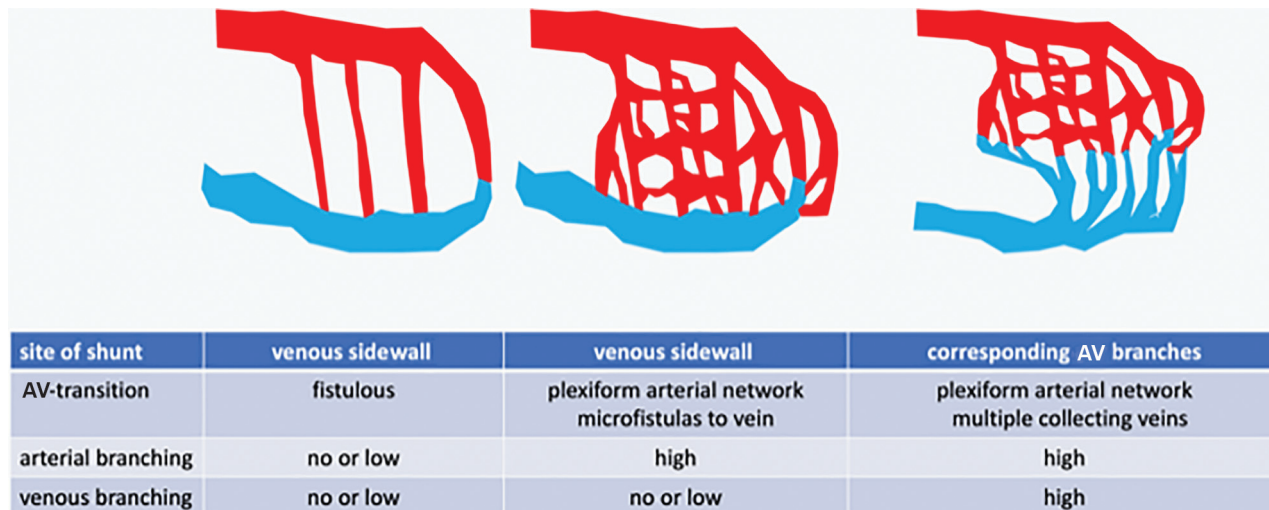


FIG 1. Schematic drawing of 4D-fPCBCTA findings in cases of AVMs to characterize different types of intranidal AV shunts and intranidal branching patterns (modified according to the classification of Houdart et al³).

- Nidus arterial: fistulous with single or multiple direct connections to a draining vein with no or a low degree of arterial branching versus a plexiform arterial network prior to the transition into the draining vein
- Nidus venous: single-versus-several draining veins/degree of venous branching with confluent collectors
- Shunt type: sidewall/corresponding arterial and venous branches
- Draining veins: single, multiple, deep, superficial, venous stenosis, varicose enlargement, venous aneurysm
- Associated aneurysms: feeding artery/intranidal/venous.

In 5 patients treated by transarterial embolization, it was possible to compare 4D reconstructions with corresponding superselective angiograms. Due to the retrospective character of this study, the results of superselective catheterization were known to the reviewers.

RESULTS

Thirty-three 4D-DSA data sets from 33 patients, 18 men and 15 women with a mean age of 40 years (range, 18–77 years), fulfilled the inclusion criteria and were evaluable. Online Supplemental Data show the AVM characteristics.

Online Supplemental Data: AVM Characteristics

4D-fPCBCTA and 2D-DSA. Angioarchitectonic features were evaluable on 4D-fPCBCTA reconstructions in all 33 cases. Twenty-six of 33 data sets were evaluable in all aspects. In 7 cases, we had problems separating the arterial and venous portions of the shunt zone due to overlapping of the angiographic phases. With 1 exception of a patient with a very small fistulous AVM, which was difficult to detect on MPR, this problem occurred in the analysis of high-flow AVMs with several feeders and tortuous draining veins that were difficult to follow on multiplanar reconstructions. Four of the total of 7 difficult to reconstruct AVM's were Spetzler-Martin grade III and IV. However, the other AVM's with Spetzler-Martin grade III and 4 could be evaluated without particular difficulty.

Simple features such as the number and course of arterial feeders and draining veins could be detected on 2D-DSA. In 16 of 33 AVMs, intranidal angioarchitecture was adequately evaluable with 2D-DSA. In the remaining 17 cases, the reviewers found that 4D-fPCBCTA provided additional findings regarding the intranidal vasculature that was obscured on projection images. In all cases, MR imaging or fusion images of MR imaging and 4D-fPCBCTA were needed to describe the exact anatomic location of the nidus and its relationship to the surrounding brain or CSF spaces.

Terminal and En Passage Feeders. Most of the AVMs had a limited number of 1–3 arterial feeders ($n = 25$). Multiple feeders were detected in 8, and extensive perinidal networks of pial arteries, in 6 cases. Twenty AVMs were supplied by a single artery or several arteries terminating in the nidus. Feeders en passage passing the AVM with small side branches to the nidus were visible in 8, and mixed patterns, in 5 cases, mostly in cases with parenchymal AVMs (Fig 3).

Intranidal Branching Patterns and Shunt Zone. 4D-fPCBCTA reconstructions detected fistulous connections with direct transition between intranidal arteries and draining veins and a low degree of arterial branching as a dominant pattern in 22 of 33 cases. In 11 patients, we observed plexiform arterial networks before the connection to the draining veins. AV shunts in the sidewall of the draining veins without or with only a few (up to 3) confluent venous branches were dominant in 19 AVMs. Shunts between corresponding arterial and venous branches of the nidus predominated in 14 AVMs with higher degrees of arterial and venous branching.

In AVMs with a single draining vein, fistulous shunts in the sidewall were detected in 15 of 24 cases. In 8 further cases with confluent branches to a single draining vein, the shunts occurred between corresponding arterial and venous branches. In 9 AVMs, we observed several draining veins with both types of AV

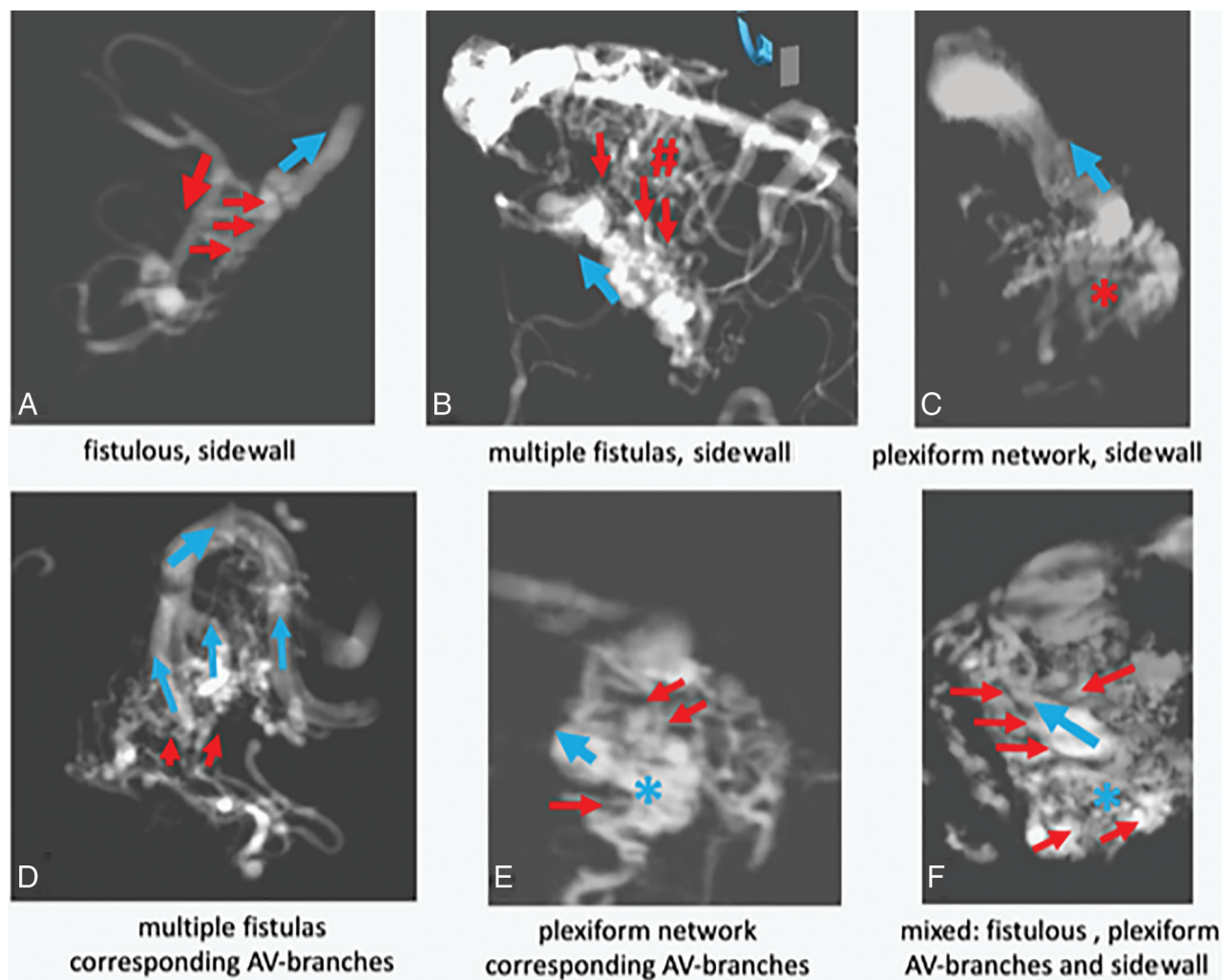


FIG 2. 4D-fPCBCTA reconstructions of the intranidal shunt zone to demonstrate different types of transitions between arterial and venous parts of the nidus in clinical cases: *A*, small AVM with several direct fistulas (small red arrows) between the feeding artery passing the nidus (large red arrow) to the sidewall of the draining vein (blue arrow). No arterial or venous branching. *B*, Multiple direct fistulas (small red arrows) to the sidewall of the tortuous draining vein (large blue arrow). Note the perinidal connections between the feeding arteries (red hashtag) in multiple fistulas, sidewall of Fig 2*B*. *C*, A plexiform arterial network (red asterisk) before multiple small shunts to the sidewall of the draining vein (blue arrow). *D*, Multiple fistulous connections between lenticulostriate arteries and corresponding branches of the thalamostriate vein in a basal ganglia AVM. *E*, A loose network of arterial branches with transition into corresponding venous branches connected to the compartmental draining vein (blue asterisk and arrow). *F*, A mixed pattern with multiple direct fistulas to the sidewall of the draining vein in the upper part of the nidus (small red arrows). A plexiform network of arterial branches with corresponding venous branches to a venous confluence (blue asterisk) connected to the draining vein (blue arrow) in the lower part of the nidus.

transitions (sidewall and confluent collecting venous branches). With the exception of 3 small fistulous AVMs with simple direct connections between the feeding arteries and veins without arterial and venous branching, mixed types between fistulous and plexiform arterial branching patterns and shunt types were observed (Table). Figure 1 shows a schematic drawing of 4D-fPCBCTA reconstructions of the different branching patterns; Fig 2 shows corresponding illustrative cases.

In 7 AVMs, different compartments with separate feeding branches and draining veins could be distinguished. Figure 3 shows a 3-compartment AVM with different branching patterns of the transitions between feeding arteries and draining veins. In this and 4 other cases, 4D-fPCTA analysis of the nidal

angioarchitecture corresponded well to the findings of superselective angiograms before embolization (Fig 4).

Associated Aneurysms

AVM-associated pre- or intranidal aneurysms were detected in 5 cases (Online Supplemental Data). All aneurysms identified with 2D-DSA were also visible on 4D-DSA reconstructions. However, a targeted search is necessary to identify small intranidal aneurysms, aneurysms on the venous side, or fusiform aneurysms in the prenidial course of a feeder. Figure 4 shows a typical example with an intranidal aneurysm close to the transition between the arterial part of the nidus and the compartmental draining vein.

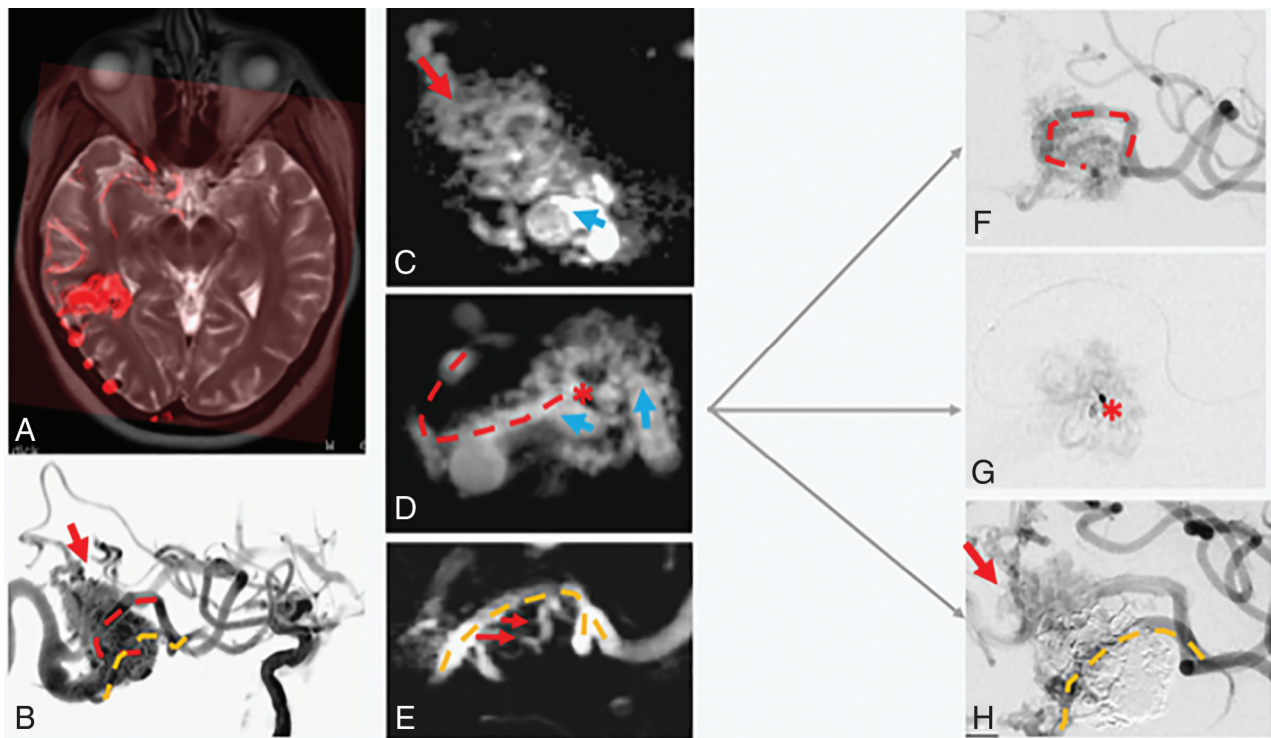


FIG 3. Angioarchitecture of the shunt zones of an AVM with a multicompartmental nidus. *A*, Fusion image between MR imaging and 4D-fPCTA shows a right, parietal, superficial AVM in a sulcus and adjacent parenchyma. *B*, 4D-volume data set presented in a virtual DSA mode with a “working projection” shows 3 main arterial feeders to the upper part of the nidus (red arrow) and to the middle (red dotted line) and lower (orange dotted line) compartments of the nidus. *C*, 4D-fPCBCTA reconstruction demonstrates the upper arterial feeder terminating in a plexiform arterial network before transition into the compartmental draining vein (blue arrow). *D*, Intracanal course of the main arterial feeder terminating in the middle compartment of the nidus (red dotted line, see also *B* and *F*). Intracanal arterial branching (red asterisk) with an arterial network and multiple small shunts in the sidewall of the draining vein (blue arrows). *E*, Another feeder passes the nidus (orange dotted line), giving off multiple side branches (small red arrows) connected to the arterial network of the nidus. *F*, 4D analysis corresponds well with 2D-DSA, with the main feeder terminating in the nidus (red dotted line). *G*, Superselective angiogram confirms the branching point to the arterial network (red asterisk). *H*, Occlusion of the compartment and the compartmental draining vein after injection of Onyx. The remaining nidus is fed by the upper feeder.

DISCUSSION

Our study confirmed findings from a first pilot project and showed that the application of 4D-DSA and 4D-fPCBCTA reconstructions for detailed analysis and classification of AVM is feasible. Compared with our first study,¹² the new software prototype provides an improved time-resolved visualization and facilitates separation between arterial and venous parts of the nidus. However, in complex AVM morphologies with several arterial feeders and draining veins, it was still difficult to follow the vessels and separate the arterial from the venous part of the nidus. As in any imaging approach for the analysis of AVM angioarchitecture, the 4D technique has limitations in the resolution of complex, overlapping vascular structures.

The simultaneous visualization of arteries and veins was not only a consequence of the AV shunt but also due to the overlap of the angiographic phases due to the scan time of 12 seconds and the requirement for a prolonged contrast bolus injected during >6 seconds to fill and visualize small vessels. Nevertheless, our method succeeded in selecting a suitable working projection and time of best filling of the nidus on virtual DSA reconstructions. Details of intracanal angioarchitecture could be visualized on time-resolved fPCBCTA MPRs in the working projection and in

the 3 standard planes with variable section thicknesses and window settings, to reduce the complexity and overlay of vessels outside the nidus,

4D technique with the reconstruction options showed advantages over conventional angiographic imaging: It was possible to obtain most of the information from time-resolved reconstructions of a single 3DRA run. Our kind of 4D data analysis provided a more detailed display of the angioarchitecture of the nidus than previous publications dealing with less complex features like the number of arterial feeders, the size of the nidus, the presence of associated aneurysms, and the number of draining veins.¹⁴⁻¹⁶ Beyond these findings, we could add more information for a detailed description of the transition between feeding arteries and the nidus, branching patterns within the shunt zone, and intracanal compartments with corresponding feeders and draining veins. Our findings met the criteria of AVM classifications and descriptions of the angioarchitecture in the literature.^{1,2,6}

Thus 4D-DSA reconstructions could differentiate between arterial feeders terminating in the nidus and feeders en passage from an artery passing the AVM for supply of normal brain tissue distal to the nidus. Mixed patterns and different lengths between

the origin and target of terminal feeders suggest that there is no strong separation between the 2 entities but a continuum between single terminal feeders with a longer distance between the last visible side branch and the nidus and AVMs fed by multiple short-distance side branches of an artery passing the nidus (en passage), with the clinical consequence that embolization with fluids is more difficult and complete obliteration of the nidus less likely.¹⁷ The presence of pial networks of collaterals between different feeding arteries has been described as perinidal angiopathy with difficulty separating the increased number and density of vessels from the nidus itself.¹⁸

Concerning the intranidal branching patterns, classifications distinguished between fistulous and plexiform compartments.¹⁸ 4D-fPCBCTA with thin slices could assign nidal compartments to one of these patterns. However, we frequently detected mixed patterns, and it was difficult to distinguish tortuous intranidal branches from real networks with anastomotic channels between adjacent vessels. Pure plexiform or simple AV fistulas were rarely seen. Our findings

represent rather a continuum with lower-to-higher degrees of branching and network formation before the AV shunt. Houdart et al³ proposed a classification for AV shunts according to the branching pattern: Arteriovenous fistulas with direct connections between arteries and a draining vein were distinguished from AV fistulas with arterial branching before transition into the draining vein and AV fistulas with corresponding branches on the venous site.

This classification provides a nomenclature that is also applicable to the description of 4D-fPCBCTA findings (Fig 1 and Table).

Venous drainage into one or several draining veins was also complex and resembled normal venous anatomy in the corresponding region. In most of our cases, 4D-fPCBCTA reconstructions were helpful in identifying the course of the compartmental draining vein and the arterial inflow to the AV shunt. These findings became important for pretherapeutic planning of transvenous embolization of AVMs, demanding control of the arterial inflow and an exact defini-

tion of the venous target and shunt zone.⁸

Details of the confluence of venous branches to the main draining veins were obscured by overlay of other nidal structures or a tortuous course of the draining veins, but time-consuming analysis taking between 30 and 60 minutes gave at least an impression of venous anatomy, which was coincident with DSA findings and superselective angiography in selected cases.

We found that flow-related pathologies like associated aneurysms and venous pathologies like stenosis or varicose enlargement can be detected quite reliably by 4D-DSA, similar to findings in other studies.¹⁴⁻¹⁶

Concerning the display of all angioarchitectonic features, 4D-DSA and fPCBCTA provide more information compared with other angiographic imaging modalities. Thus, planning of interventional, surgical, and radiosurgical treatment may benefit from improved characterization of the nidus and the shunt zone. Conventional 2D-DSA showed most

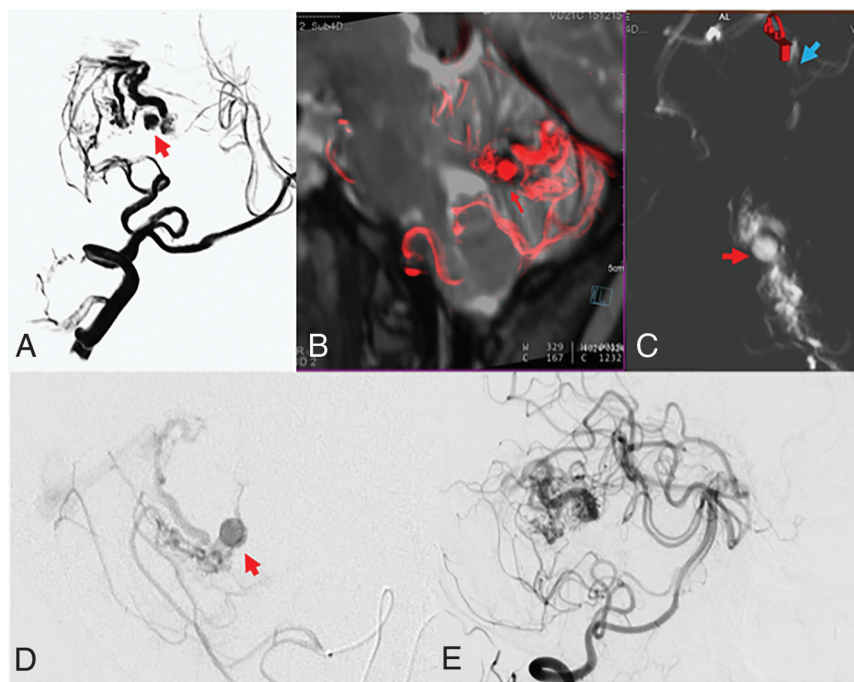


FIG 4. Posterior fossa AVM in an 18-year-old woman with cerebellar hemorrhage. A and B, Virtual DSA and sagittal reconstructions of fused images between MR imaging and 4D fPCBCTA show an intranidal aneurysm (red arrows). C, Axial MPRs demonstrate the origin of the aneurysms from the branches of the small nidus just proximal to the transition into the draining vein (blue arrow). D, Corresponding findings by superselective angiography. E, Occlusion of the aneurysm after targeted embolization. Note the diffuse nidus with a low degree of branching and dominance of single microfistulous channels.

Intranidal branching pattern and venous drainage

Venous Drainage	Dominant Arterial Branching Pattern		Dominant Shunt Type	
	Direct Fistulas	Plexiform Network	Sidewall	AV Branching
Single draining vein (n = 24)	17	7	15	8
Several draining veins (n = 9)	5	4	4	6
Total (n = 33)	22	11	19	14

of the findings with the advantage of better temporal resolution and separation between the angiographic phases. At the current stage of development of 4D technology, DSA projection images are still needed as complementary information. 4D with the advantage of displaying the volumes at any time point in any projection may help avoid DSA series in multiple projections or high frame rates. The main disadvantage of DSA was the overlay of vascular structures on projection images. Further prospective and multicentric studies are necessary to assess whether additional oblique 2D-DSA projections can be omitted without loss of diagnostic quality.

With the use of subtraction, soft-tissue contrast is not shown in 3D and 4D reconstructions. Therefore, display of gray and white matter gyri and sulci of the brain is not possible. Soft-tissue reconstruction algorithms for the mask are available and may also be used for C-like fPCBCT images. Currently, the resolution for soft-tissue details like the differentiation between gray and white matter is less than that with multislice CT or MR imaging. Therefore, MR imaging or fusion images between 4D-fPCBCTA and MR imaging became necessary for the exact localization of the AVM nidus and its relationship to the brain parenchyma and adjacent CSF spaces in our study.

Our study had several limitations:

1) The retrospective character with a limited number of 33 consecutive cases may be associated with a risk of bias towards certain AVM types and locations.

2) The analyses and ratings were performed with awareness of the findings of other imaging modalities. To demonstrate the validity of the new method, further prospective studies with blinded reviewers are necessary. At the current stage of software development, analyses were still time-consuming and difficult to standardize, especially in larger AVMs with complex angioarchitecture. Automated vessel-tracking algorithms and slice selection according to fused volumes between MRI and 4D-fPCTA should be developed to facilitate the determination of the AVM site and angioarchitectonic features.

3) According to our institutional rules, 3DRA in patients with AVM was only indicated if treatment was considered. This practice explains a predominance of small, ruptured AVMs in our sample, which is probably not representative.

4) In AVMs with feeders from different arterial territories, the analysis of 4D data obtained by injection of 1 feeder may not cover all compartments of the nidus. Image fusion could put the data from several 4D-DSA volumes together, with the disadvantage of increasing radiation exposure.

5) Details of the shunt zone could be confirmed by super-selective angiography. In our sample, this information was only available in selected patients who underwent superselective embolization.

6) Despite suggestions to establish a standardized reporting terminology,² there is still a lack of validated categories for a description of angioarchitecture details. 4D-fPCBCTA reconstructions are able to display the continuum between known subtypes and may contribute to in vivo evaluation of this complex disease.

CONCLUSIONS

4D-DSA reconstructions are superior to 2D-DSA for displaying pathoanatomic details concerning angioarchitecture and classification of cerebral AVMs. At the current stage of development, DSA projection images and MR imaging are still needed as complementary diagnostic tools. Future 4D-fPCBCTA may play an important role as tool for pretherapeutic assessment of brain AVMs as well as a research tool for display of the intra- and perinidal microvasculature. Further standardization of postprocessing and improvement of fPCTA MR imaging fusion are necessary for further studies with blinded reviewers.

Disclosure forms provided by the authors are available with the full text and PDF of this article at www.ajnr.org.

REFERENCES

1. Müller-Forell W, Valavanis A. **How angioarchitecture of cerebral arteriovenous malformations should influence the therapeutic considerations.** *Minim Invas Neurosurg* 1995;38:1430–42 [CrossRef Medline](#)
2. Atkinson RP, Awad IA, Batjer HH, et al; Joint Writing Group of the Technology Assessment Committee American Society of Interventional and Therapeutic Neuroradiology; Joint Section on Cerebrovascular Neurosurgery a Section of the American Association of Neurological Surgeons and Congress of Neurological Surgeons; Section of Stroke and the Section of Interventional Neurology of the American Academy of Neurology. **Reporting terminology for brain arteriovenous malformation: clinical and radiographic features for use in clinical trials.** *Stroke* 2001;32:1430–42 [CrossRef Medline](#)
3. Houdart E, Gobin YP, Casasco A, et al. **A proposed angiographic classification for intracranial arteriovenous fistulae and malformations.** *Neuroradiology* 1993;35:381–85 [CrossRef Medline](#)
4. Berenstein AL, ter Brugge KG. **Clinical and Endovascular Treatment Aspects in Adults.** In: Berenstein AL, Lasjaunias P, ter Brugge KG, *Surgical Neuroangiography*. Vol 2.1. 2nd ed. Springer-Verlag; 2004
5. Yasargil MG. *Microneurosurgery, Vol 4: AVM of the Brain, History, Embryology, Pathological Considerations, Hemodynamics, Diagnostic Studies, Microsurgical Anatomy*, Thieme; 1987
6. Orłowski P, Mahmud I, Kamran M, et al. **An approach to the symbolic representation of brain arteriovenous malformations for management and treatment planning.** *Neuroradiology* 2014;56:195–209 [CrossRef Medline](#)
7. Mohr JP, Parides MK, Stapf C, et al; International ARUBA Investigators. **Medical management with or without interventional therapy for unruptured brain arteriovenous malformations (ARUBA): a multicentre, non-blinded, randomised trial.** *Lancet* 2014;383:614–21 [CrossRef Medline](#)
8. Choudhri O, Ivan ME, Lawton MT. **Transvenous approach to intracranial arteriovenous malformations: challenging the axioms of arteriovenous malformation therapy?** *Neurosurgery* 2015;77:644–52 [CrossRef Medline](#)
9. Al-Shahi R, Pal N, Lewis SC, et al; Observer Agreement Study Group. **Agreement in the angiographic assessment of arteriovenous malformations of the brain.** *Stroke* 2002;33:1501–09 [CrossRef Medline](#)
10. Spetzler RF, Ponce FA. **A 3-tier classification of cerebral arteriovenous malformations.** *J Neurosurg* 2011;114:842–49 [CrossRef Medline](#)
11. Dumont TM, Kan P, Snyder KV, et al. **A proposed grading system for endovascular treatment of cerebral arteriovenous malformations: Buffalo score.** *Surg Neurol Int* 2015;6:3 [CrossRef Medline](#)
12. Lescher S, Gehrisch S, Klein S, et al. **Time-resolved 3D-rotational angiography display of detailed neurovascular anatomy in patients**

- with intracranial vascular malformations. *J Neurointerv Surg* 2017;9:887–94 [CrossRef Medline](#)
13. Tritt S, Ommer B, Gehrisch S, et al. Optimization of the surgical approach in AVMs using MRI and 4D DSA fusion technique. *Clin Neuroradiol* 2017;27:443–50 [CrossRef Medline](#)
 14. Lang S, Gölitz P, Struffert T, et al. 4D DSA of dynamic visualization of cerebral vasculature: a single-center experience in 26 cases. *AJNR Am J Neuroradiol* 2017;38:1169–76 [CrossRef Medline](#)
 15. Ognard J, Magro E, Caroff J, et al. A new time-resolved 3D angiographic technique (4D-DSA): description, and assessment of its reliability in Spetzler-Martin grading of cerebral arteriovenous malformations. *J Neuroradiol* 2018;45:177–85 [CrossRef Medline](#)
 16. Sandoval-Garcia C, Royalty K, Yang P, et al. 4D DSA a new technique for arteriovenous malformation evaluation: a feasibility study. *J Neurointerv Surg* 2016;8:300–04 [CrossRef Medline](#)
 17. Geibprasert S, Pongpech S, Jiarakongmun P, et al. Radiologic assessment for brain arteriovenous malformations: what clinicians need to know. *Radiographics* 2010;30:483–501 [CrossRef Medline](#)
 18. Valavanis A, Pangalu A, Tanaka M. Endovascular treatment of cerebral arteriovenous malformations with emphasis on the curative role of embolization. *Interv Neuroradiol* 2005;11:37–43 [CrossRef Medline](#)